Agonist-activated Ca^{2+} influx occurs at stable plasma membrane and endoplasmic reticulum junctions

Susan Treves[1,2], Mirko Vukcevic[1], Johanna Griesser[1], Clara-Franzini Armstrong[3], Michael X. Zhu[4] and Fancesco Zorzato[1,2,*]

[1]Departments of Anesthesia and Biomedizin, Basel University Hospital, Basel, Switzerland
[2]Dipartimento di Medicina Sperimentale e Diagnostica, sez Patologia Generale, University of Ferrara, Via Borsari 46, 44100 Ferrara, Italy
[3]Department of Cell/Developmental Biology, University of Pennsylvania, Philadelphia, PA 19104, USA
[4]Department of Neuroscience, Biochemistry, and Center for Molecular Neurobiology, The Ohio State University, Columbus, OH 43210, USA
*Author for correspondence (zor@unife.it)

Accepted 12 August 2010
Journal of Cell Science 123, 4170-4181

doi:10.1242/jcs.068387

Summary

Junctate is a 33 kDa integral protein of sarco(endo)plasmic reticulum membranes that forms a macromolecular complex with inositol 1,4,5-trisphosphate [Ins(1,4,5)P_3] receptors and TRPC3 channels. TIRF microscopy shows that junctate enhances the number of fluorescent puncta on the plasma membrane. The size and distribution of these puncta are not affected by the addition of agonists that mobilize Ca^{2+} from Ins(1,4,5)P_3-sensitive stores. Puncta are associated with a significantly larger number of peripheral junctions between endoplasmic reticulum and plasma membrane, which are further enhanced upon stable co-expression of junctate and TRPC3. The gap between the membranes of peripheral junctions is bridged by regularly spaced electron-dense structures of 10 nm. Ins(1,4,5)P_3 inhibits the interaction of the cytoplasmic N-terminus of junctate with the ligand-binding domain of the Ins(1,4,5)P_3 receptor. Furthermore, Ca^{2+} influx evoked by activation of Ins(1,4,5)P_3 receptors is increased where puncta are located. We conclude that stable peripheral junctions between the plasma membrane and endoplasmic reticulum are the anatomical sites of agonist-activated Ca^{2+} entry.

Key words: Puncta, TIRF, Peripheral junctions, Calcium

Introduction

In excitable and non-excitable cells, activation of Ca^{2+} release from stores present in the endoplasmic or sarcoplasmic reticulum is accompanied by Ca^{2+} influx from the extracellular environment, a fundamental step that is necessary to replenish intracellular stores and allow cells to respond to successive stimulatory signals (Feske et al., 2001; Putney, 2007; Berridge, 2004; Parekh and Putney, 2005; Eisner and Trafford, 2009). In non-excitable cells, the molecular mechanism involved in store-operated Ca^{2+} entry (SOCE) has been extensively investigated and a number of molecules have been shown to be involved in Ca^{2+} influx (Wu et al., 2007; Putney, 2007). The most popular candidates expressed in most mammalian cells are STIM1 (stromal interaction molecule 1) and Orai1 (calcium-release-activated calcium channel protein 1). STIMs are proteins that contain a single transmembrane domain and a luminal N-terminal domain endowed with an EF hand that functions as a Ca^{2+} sensor in the lumen of the endoplasmic reticulum (ER) (Liou et al., 2005; Zhang et al., 2005; Stathopulos et al., 2006; Spassova et al., 2006; Huang et al., 2006); Orai1 is the pore-forming unit of the SOCE channel (Gwack et al., 2007; Prakriya et al., 2006; Yeromin et al., 2006). When intracellular Ca^{2+} stores are full, STIM1 proteins are diffusely distributed in the ER as monomers, but upon store depletion, STIM1 undergoes conformational changes resulting in oligomerization and redistribution into puncta located 10–25 nm from the plasma membrane (PM) (Luik et al., 2008; Vig et al., 2006; Wu et al., 2006; Park et al., 2009). Orai1 proteins are then recruited to STIM-containing puncta, whereby they form a complex and reconstitute functional Ca^{2+} influx channels (Wu et al., 2007; Park et al., 2009; Penna et al., 2008). The time frame of STIM1 relocalization is in the order of hundreds of seconds (Wu et al., 2006) and appears to be of the same order of magnitude of the peak inward Ca^{2+} current via I_{CRAC} (Hofer et al., 1998; Wu et al., 2006). However, recent studies have suggested that SOCE is a complex mechanism that might require additional components (Varnai et al., 2007; Gwozdz et al., 2008).

Agonist-mediated generation of inositol 1,4,5-trisphosphate [Ins(1,4,5)P_3] induces inositol 1,4,5-trisphosphate receptor (InsP_3R)-dependent Ca^{2+} release from intracellular stores, and this is followed by sustained Ca^{2+} entry, an event known as agonist-activated Ca^{2+} entry (Berridge, 1995). This is mediated by the influx of extracellular Ca^{2+} via receptor- and/or store-operated Ca^{2+} channels localized on the PM. In principle, agonist-activated Ca^{2+} entry could be a secondary event, mediated by the depletion of InsP_3-sensitive stores, resulting in the activation of SOCE. However, experimental data indicate that agonist-activated Ca^{2+} entry is functionally distinct from SOCE; in fact, Van Rossum and co-workers (Van Rossum et al., 2004) have shown that agonist-activated Ca^{2+} entry occurs in DT40 cells expressing InsP_3R mutants that are unable to release Ca^{2+} from the ER, but are capable of interacting with their ligand, InsP_3, although these data have stirred some controversies (Vazquez et al., 2002; Dellis et al., 2006). If the InsP_3R is the only intracellular Ca^{2+} channel of DT40 cells, these data have two important implications. First, stimulation of agonist-activated Ca^{2+} entry might occur without store depletion and without the translocation of ER membrane domains from the cytosol to the subplasmalemmal space. Second, Ca^{2+} entry is activated by the interaction of InsP_3 with InsP_3Rs and this interaction in turn induces a conformational coupling between InsP_3Rs and Ca^{2+} entry channels, via a mechanism similar to that involved in muscle excitation–contraction coupling. The anatomical site of muscle excitation–contraction coupling is

Journal of Cell Science

the calcium release unit (CRU) (Franzini-Armstrong and Jorgensen, 1994; Franzini-Armstrong and Protasi, 1997), which contains ordered arrays of ryanodine receptor Ca^{2+} release channels coupled to L-type voltage-dependent Ca^{2+} channels. CRUs might be formed by a stable and direct association of the sarcoplasmic reticulum with the PM (peripheral couplings, mostly found in developing muscles) or by the association of two to three elements, a transverse T tubule, and one or two closely apposed terminal cisternae of the sarcoplasmic reticulum (triads and diads, representing mature CRUs) (Franzini-Armstrong and Protasi, 1997). Interestingly, it was recently shown that in skeletal muscle, Junctophilin-1, a 72 kDa membrane-spanning protein, mediates the physical linkage of transverse tubules to the SR membrane (Takeshima et al., 2000; Weisleder et al., 2008).

Experimental evidence indicates that the structural requirements for SOCE and agonist-activated Ca^{2+} entry are substantially different. In the first case, store depletion induces long-range dynamic interactions between the ER membrane and the PM, leading to the formation of ER–PM junctions; the formation of such transient junctions allows the functional coupling between STIM1 and Orai1 (Park et al., 2009). The agonist-activated Ca^{2+}-entry model, however, predicts the existence of pre-formed ER–PM junctions without the requirement of store depletion during receptor-mediated signal transduction (Berridge, 2004). ER–PM junctions might be a macromolecular complex, which contains, in addition to InsP_3R and Ca^{2+} influx channels, scaffold proteins modulating the functional interaction between the InsP_3R and the Ca^{2+}-entry channel (Kiselyov et al., 2005). Understanding of the structural organization of the molecular components involved in Ca^{2+} entry is important to define the mechanism(s) by which Ca^{2+} entry is physiologically activated.

To investigate the mechanism(s) involved in modulation of Ca^{2+} entry, we studied the relationship between the structural and functional properties of the supramolecular complex involved in Ca^{2+} entry, which is composed of junctate (one of the splice variants encoded by the ASPH locus), the short transient receptor potential channel TRPC3 and InsP_3R (Treves et al., 2000; Treves et al., 2004). Here, we show that in HEK293 cells stably transfected with junctate–YFP, junctate distributes in the ER as well as in discrete puncta on the plasma membrane, and the latter correlate with the appearance of peripheral couplings between the ER and the PM. The number of ER–PM peripheral couplings is further increased by co-expression of junctate and TRPC3 channels. Interestingly, the gap of the peripheral couplings is regularly occupied by electron-dense structures of 10 nm. TIRF microscopy demonstrates that junctate-containing puncta are involved in agonist-mediated Ca^{2+} influx. Contrary to what has been observed for STIM1, however, activation of Ca^{2+} release from the ER does not result in a rapid movement or redistribution of the junctate-containing ER to the PM. Based upon these results we conclude that agonist-activated Ca^{2+} entry might also occur at stable ER–PM junctions endowed with junctate and other components of the supramolecular complex mediating Ca^{2+} influx, including TRPC3 channels and InsP_3R.

Results

Peripheral couplings between endoplasmic reticulum and plasma membrane in stable clones of HEK293 cells expressing junctate–YFP

Junctate is a scaffold protein which might be involved in the assembly of peripheral junction between the PM and the ER by forming a supramolecular complex with InsP_3Rs and the Ca^{2+}-influx channel TRPC3 (Treves et al., 2000; Treves et al., 2004; Kiselyov et al., 2005) (supplementary material Fig. S1). In the first set of experiments, we examined whether peripheral couplings are endowed with some of the components making up the junctate–InsP_3R–TRPC3 supramolecular complex. For this investigation we obtained stable HEK293 clones expressing the junctate–YFP fusion protein. We screened several clones expressing varying amounts of junctate–YFP and the major functional properties of clone 21 are summarized in Fig. 1. The expression of the junctate–YFP fusion protein was evaluated by western blot analysis using anti-GFP antibodies (Fig. 1A, left). Fig. 1 also shows that the major InsP_3R isoform expressed in our HEK293 cells was type 3 and chronic overexpression of junctate was associated with a significant increase in its level of expression as determined by western blotting and real-time RT-PCR (Fig. 1A). The absence of immunoreactive bands with antibodies against type 1 and 2 InsP_3R in HEK293 microsomes was not due to the lack of reactivity of the antibodies because control western blots on mouse brain microsomes were positive (results not shown). We next monitored global intracellular Ca^{2+} homeostasis by assessing the size of agonist- and thapsigargin-sensitive Ca^{2+} stores of clone 21 in a population of Fura-2-loaded cells. Overexpression of junctate is associated with significantly larger global peak Ca^{2+} transients in response to the addition of ATP, a purinergic receptor agonist that triggers InsP_3 production, or to 400 nM of the SERCA inhibitor thapsigargin (Fig. 1B). Overexpression of junctate did not significantly affect the resting [Ca^{2+}], because the mean Fura-2 resting fluorescence ratios of HEK293 cells and clone 21 cells were similar (1.14±0.02 and 1.11±0.02 in 12 and 10 independent measurements, respectively).

We next examined whether the junctate–YFP recombinant fusion protein is localized within a space that is 100–150 nm from the PM. We performed such analysis by TIRF microscopy, a technique that offers higher spatial resolution (150 nm) compared with that offered by conventional confocal microscopy. Fig. 1C shows bright-field images (left panels) and epifluorescence images of HEK junctate–YFP stable clones (top left) or HEK293 cells transiently transfected with a plasmid encoding SScalEGFP (bottom left), a recombinant protein that is targeted to the ER, and is comprised of a signal sequence, followed by GFP and KDEL at its C-terminus. As seen by epifluorescence (Fig. 1C, central panels), the fluorescent patterns of junctate–YFP and SScalEGFP were virtually identical, radiating from the perinuclear area towards the PM in a mesh-like pattern. When the focal plane was fixed to the interface of glass coverslip with the cell membrane using a surface reflection interference contrast filter (SRIC cells, Fig. 1C, right panels) and cells were viewed by TIRF microscopy (488 nm excitation), the fluorescent patterns were significantly different. In fact, junctate–YFP appeared as discrete fluorescent puncta (Fig. 1D, top), whereas the GFP fusion protein targeted to the ER had a worm-like appearance on discrete areas of the PM (Fig. 1D, bottom). The size and shapes of the fluorescent particles were analyzed in greater detail and are summarized in Table 1, the length and radius of the junctate–YFP particles was significantly smaller than those observed in SScalEGFP-transfected cells; furthermore, the shape factor (1.0 is the value of a circle) of the puncta in junctate–YFP-transfected cells was 0.94 and significantly higher than that obtained in SScalEGFP-transfected cells. We also investigated whether the InsP_3R3 in HEK junctate–YFP cells colocalizes in a domain close to the plasma membrane. Detailed analysis by TIRF microscopy

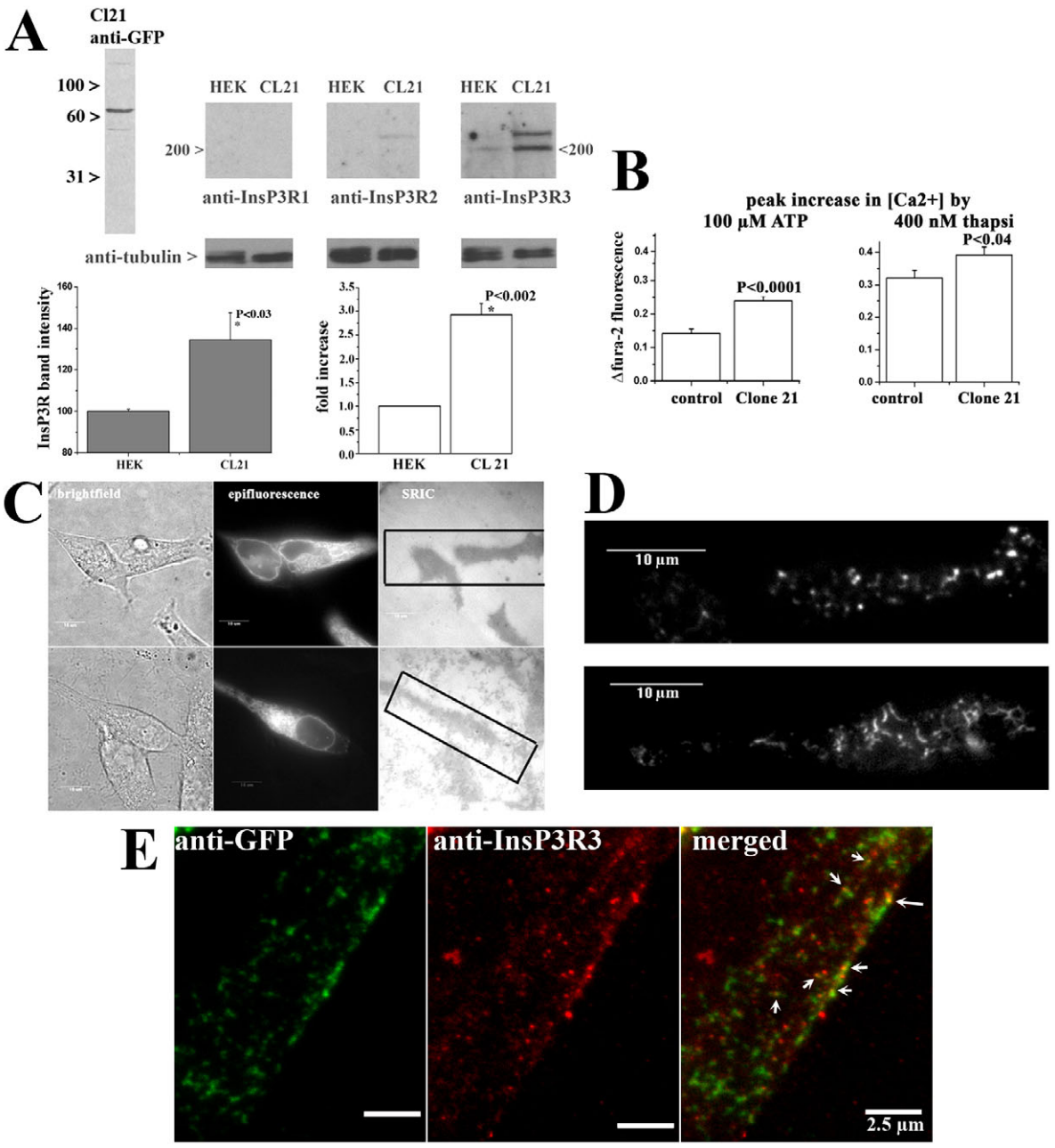

Fig. 1. Characterization of HEK clone 21 stably overexpressing junctate–YFP. (**A**) The total cell extract of clone 21 (CL21) was resolved by 10% SDS-PAGE, blotted onto nitrocellulose and probed with mouse anti-GFP (left). Microsomal proteins (50 µg/lane) from HEK293 cells or HEK CL21 cells were separated by 7.5% SDS-PAGE, blotted onto nitrocellulose and incubated with the indicated anti-InsP_3R antibody. Control for equal loading was performed by probing the blot with anti-tubulin antibodies. The histograms on the left show the mean intensity of the immunopositive bands corresponding to the lower InsP_3R3 band (corrected for β-tubulin content). Bars represent means of five experiments ± s.e.m. The histograms on the right show the relative content of InsP_3R3 transcript as assessed by real-time RT-PCR (mean ± s.e.m. of three experiments). (**B**) HEK293 junctate–YFP clone 21 cells were loaded with the fluorescent Ca^{2+} indicator Fura-2 and the peak Ca^{2+} transient obtained after addition of 100 µM ATP or 400 nM thapsigargin was determined in Ca^{2+}-free Krebs-Ringer containing 0.5 mM EGTA. Results represent the mean (±s.e.m.) peak fluorescence increase (peak ratio – resting ratio) of 1×10^6 cells/ml (n=5–6 independent determinations). (**C**) HEK293 junctate–YFP (clone 21, top) or HEK cells transiently transfected with the ER-tagged fluorescent protein SScalEGFP (bottom) were visualized under bright-field illumination (left), by epifluorescence (central), with a SRIC filter to identify the coverslip cell contact site (right) or by TIRF (**D**) at the focal plane identified with the SRIC filter. Top panel shows membrane fluorescence of HEK junctate–YFP cells showing that the fluorescence on the PM appears as distinct puncta, whereas cells expressing the ER-targeted GFP fusion protein show a ‘wormlike’ fluorescence on some areas of the PM. (**E**) Indirect immunofluorescence analysis of junctate and InsP_3R3 in HEK junctate–YFP cells. Cells were incubated with goat anti-InsP_3R3 followed by anti-goat DyLighte Fluor-405 and rabbit anti-GFP Alexa Fluor 488. The focal plane next to the plasma membrane was identified with the SRIC filter and GFP fluorescence was visualized through a 100× TIRF objective. For detection of the InsP_3R, excitation was at 405 nm and emission was visualized at 427 nm using a brightline HC 427/10 filter. Images were merged using the Metamorph software and overlapping pixels (arrows) are shown in orange.

Table 1. Shape analysis of PM fluorescent particles in HEK clone 21 and in cells overexpressing the ER-resident protein SScalEGFP

	Shape factor	Particle length (μm)	Radius (μm)
Junctate–YFP	0.94±0.014* (*n*=402)	1.30±0.03* (*n*=402)	0.38±0.01** (*n*=402)
SScalEGFP	0.84±0.028 (*n*=326)	1.67±0.10 (*n*=326)	0.456±0.03 (*n*=326)

*P<0.001; **P<0.02.

(*n*=21 cells) showed that within the area positive for YFP fluorescence, 19.4±1.3 % was also positive for InsP_3R3, and within the area positive for InsP_3R3, 15.5±1.1% was also positive for GFP (Fig. 1E). These results indicate that a small percentage of junctate and InsP_3R3 colocalize in a domain closely adjacent to the PM.

The localization and distribution of junctate–YFP puncta does not change upon agonist- induced mobilization of intracellular calcium stores

It is now well established that store-depletion activation of calcium entry (SOCE) depends on the relocalization of STIM1 from the 'whole' ER to a domain of the ER in close proximity to the PM. We examined by TIRF microscopy whether ER containing junctate–YFP similarly relocalizes to the PM during agonist stimulation. To avoid artefacts linked to minimal changes of the focal plane during time-lapse recording in the TIRF mode, we equipped our microscope with an on-line focus control. Addition of 100 μM ATP to HEK293 Cl21 cells did not affect the distribution, the appearance or the movement of the junctate–YFP puncta (Fig. 2A, *t*=0 to *t*=180 seconds). The area covered by the fluorescent puncta during stimulation with Krebs-Ringer alone or Krebs-Ringer containing 100 μM ATP were not significantly different (0.017±0.0001 and 0.015±0.0001 μm^2; 35 puncta and 43 puncta from four and five different experiments, respectively). Similarly, we did not observe relocalization of the fluorescent signal due to SScalEGFP, an artificial ER-resident protein (Fig. 2B) in transfected HEK293 cells after the addition of 100 μM ATP. If junctate–YFP-containing puncta are stably localized within a space which is 100–150 nm from the PM, one would expect that the appearance of stable puncta should be associated with an increase of peripheral junctions between the ER and the PM in cells overexpressing junctate. We tested this idea by performing transmission electron microscope analysis of junctate–YFP-expressing clones. Fig. 2C shows electron micrographs of the cell periphery in HEK junctate–YFP cells and the arrows indicate areas of contact between the PM and the ER. Where the ER membrane was parallel to the plasma membrane, the gap between the two membranes was 10.4±2.9 nm (mean ± s.d., from 13 junctions, 84 measurements). The width was not significantly different from that of HEK293 cells (9.4±3.4 nm from 38 junctions, 229 measurements). A variable portion of the gap (Fig. 2C) was regularly occupied by electron-dense structures of ~20 nm in width and 10 nm in height, which bridge the junctional gap (Fig. 2C, small arrows). Table 2 summarizes the statistical analysis of the number and size of junctions in sectioned profiles of cells. The length of the junctions in HEK293 cells and in the same cells stably expressing junctate–YFP was not significantly different (0.144±0.023 vs 0.159±0.009 μm, respectively); however, the number of junctions per sectioned profile in junctate–YFP-expressing cells was increased by almost threefold (0.092±0.031 vs 0.270±0.053) compared with YFP-expressing clones.

Enhanced ER–PM junction formation by expression of two components of the InsP_3R–TRPC3 supramolecular complex

The previous set of data suggests that the appearance of puncta and peripheral junctions is enhanced by imposing high levels of expression of junctate, one of the molecular components of the InsP_3R–TRPC3 supramolecular complex. If this is true, we reasoned that overexpression of more than one of the components of this supramolecular complex might result in a further increase of ER to plasma membrane peripheral junctions. We set out to verify this hypothesis by analyzing the structural properties of HEK cell clones stably overexpressing both TRPC3 and junctate (clone D6) and comparing them with those of clones overexpressing junctate–YFP. Semiquantitative RT-PCR of HEK (Fig. 3A) clone D6 shows that the level of mRNA encoding junctate was higher than that in HEK Cl28 control cells (HEK-T3 cells transfected with the empty pcDNA 3.1/Hygro plasmid); detailed analysis by real-time RT-PCR revealed that the level of expression of junctate was highest in clone 21, followed by clone D6 (Fig. 3C). Electron microscopy images of junctate–TRPC3-overexpressing clone D6 are shown in Fig. 3D and Table 2 summarizes results obtained on the number and size of junctions in all the HEK clones analysed. Similarly to what was observed in stable clones overexpressing junctate–YFP alone, the presence of both proteins did not significantly affect the average length of the PM–ER peripheral junctions, even though some particularly long junctions were observed (Fig. 3D). The junctional gap width (10.0±3.3 nm, from junctate–TRPC3 HEK cells, 211 measurements) was also not significantly different from either HEK or HEK junctate–YFP cells; however, the number of junctions in those cells overexpressing junctate and TRPC3 was four times higher than in those cells overexpressing junctate alone (Table 2). These data strongly suggest that the expression of the components forming the junctate–InsP_3R–TRPC3 supramolecular complex stabilizes the association between the ER and the PM, but does not alter their structure.

Stable ER–PM peripheral junctions might represent anatomical sites that are responsible for entry of extracellular Ca^{2+} into the cytoplasm and thus replenishment of intracellular Ca^{2+} stores occurring after agonist stimulation of InsP_3R. Fig. 3E shows experiments conducted in HEKT3 D6 (junctate +TRPC3 overexpressing cells): addition of 2 mM Ca^{2+} in the absence of an InsP_3-stimulating agonist did not result in Ca^{2+} influx (Fig. 3Ea, small arrow), whereas addition of Ca^{2+} in the presence of ATP (Fig. 3Eb, large arrow) resulted in a robust Ca^{2+} increase. We have previously shown that overexpression of junctate in combination with the TRPC3 entry channel is accompanied by larger intraluminal Ca^{2+} content, which can be mobilized by the addition of either 400 nM thapsigargin or 100 μM ATP (Treves et al., 2004) (supplementary material Fig. S2)

Although HEK293 clones 21 and D6 have a larger number of ER–PM junctions compared with control cells and because we

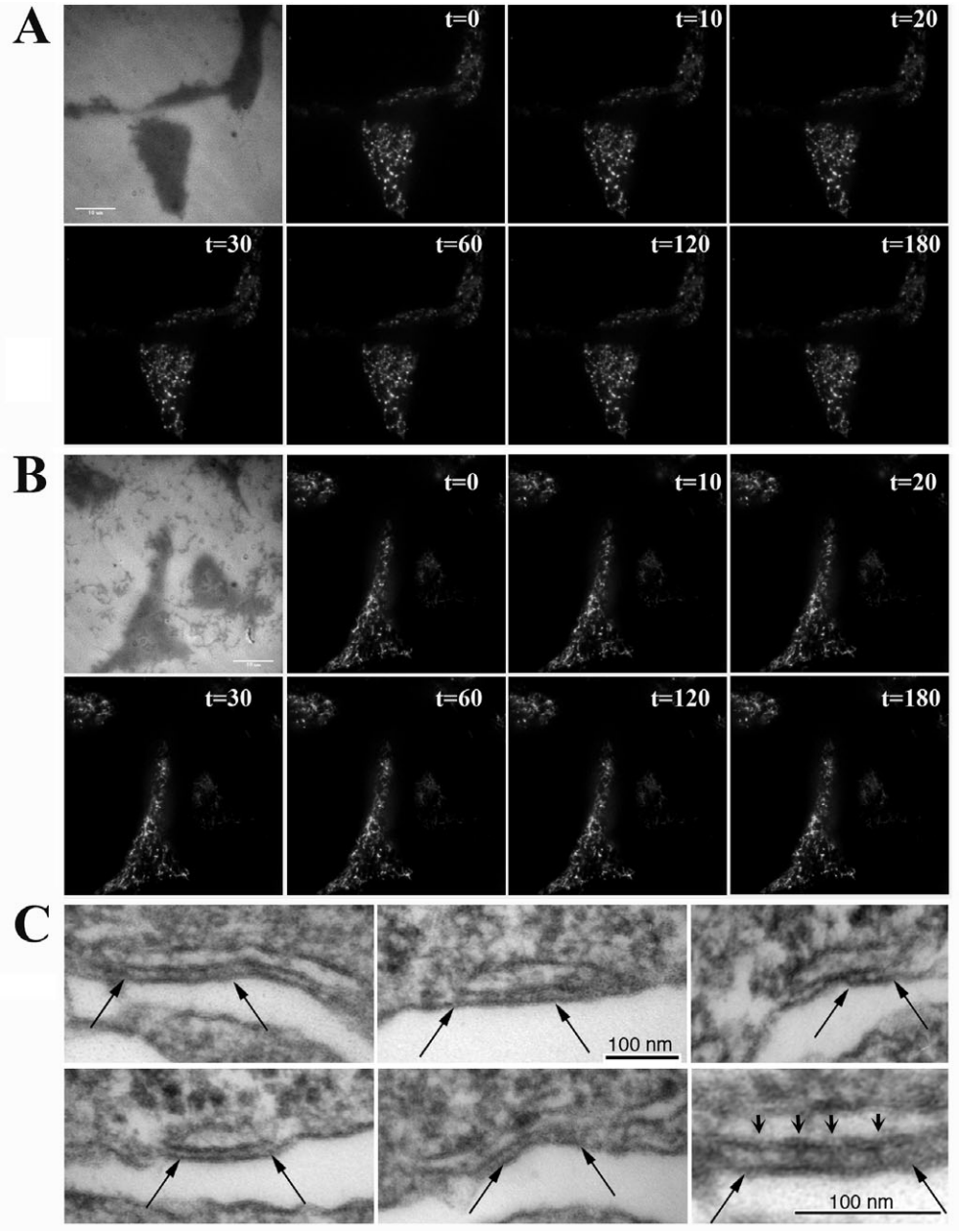

Fig. 2. HEK293 junctate–YFP cells show discrete puncta on the plasma membrane and exhibit increased number of ER–PM junctions. (**A**) HEK-junctate–YFP cells were visualized with a SRIC filter (top left panel) and then by TIRF microscopy. Panels show successive time-lapse series of the same cells after stimulation with 100 μM ATP in Krebs-Ringer containing 2 mM Ca^{2+}. (**B**) As for A, except that HEK cells were transiently transfected with the ER-resident protein SScalEGFP. Note the absence of movement of the puncta. Cells were visualized with a 100× TIRF objective (1.49 NA) and were illuminated with a Sapphire laser. Scale bar: 10 μm. (**C**) Peripheral couplings in junctate–YFP clones. Electron micrographs showing that the endoplasmic reticulum and plasma membrane form junctions (between arrows) of variable length.

consistently failed to observe Ca^{2+} entry in the absence of the InsP_3R agonist ATP (Fig. 3Ea), it seems that junctate modulates receptor-activated Ca^{2+} entry only in the presence of InsP_3. Indeed, previous reports have demonstrated that agonist-mediated Ca^{2+} entry requires the interaction of the InsP_3R with its ligand (Van Rossum et al., 2004). Since junctate can bind to InsP_3R and TRPC3 to form the junctate–InsP_3R–TRPC3 supramolecular complex, it is plausible that the lack of substantial Ca^{2+} entry in the absence of InsP_3 generation is due either to the interaction of the junctate N-terminus with a domain of the InsP_3R involved in ligand binding, or to the inhibitory interaction of junctate with the TRPC3 channel. To discriminate between these two possibilities we mapped the binding site for junctate on the InsP_3R.

Identification of the domain on the InsP_3R involved in the interaction with the junctate N-terminal domain

In vitro transcribed and translated overlapping fragments of [^{35}S]Met-labelled human InsP_3R3 (Fig. 4A) were synthesized and incubated with streptavidin-coupled beads coated with a biotinylated peptide encompassing the N-terminus of junctate (Fig.

Table 2. Peripheral couplings in HEK293 cell clones overexpressing junctate

Cell type	Average length of junctions (mean ± s.d.)	Number of junctions per cell section
HEK293 cells	144±91 nm (*n*=15 cells)	0.09 (*n*=157 cells)
HEK Junctate–YFP	159±76 nm (*n*=73 cells)	0.27 (*n*=272 cells)*
HEK TRPC3–junctate	161±76 nm (*n*=173 cells)	1.19 (*n*=149 cells)**

Student's *t*-test vs HEK293 cells: *P<0.007, **P<0.000001.

4B), the N-terminus of aspartyl-β-hydroxylase (Fig. 4C) or an unrelated peptide (Fig. 4D). Only beads that had been coated with the peptide encompassing the N-terminus of junctate interacted with recombinant InsP_3R fragments. In particular, the N-terminus of junctate pulled down construct F1, which encompasses the InsP$_3$R domain involved in ligand (InsP_3) binding, as well as construct F4, which encompasses residues 1391–2249. A faint band indicating binding to construct F3 (residues 1119–1460) was also visible. The N-terminus of aspartyl-β-OH failed to interact with constructs F1–F5, as did the unrelated peptide.

We next verified whether the N-terminus of junctate bound within the same domain involved in ligand binding, by performing pull-down experiments in the presence of increasing concentrations of InsP_3. For this assay, we tested InsP_3 concentrations that are

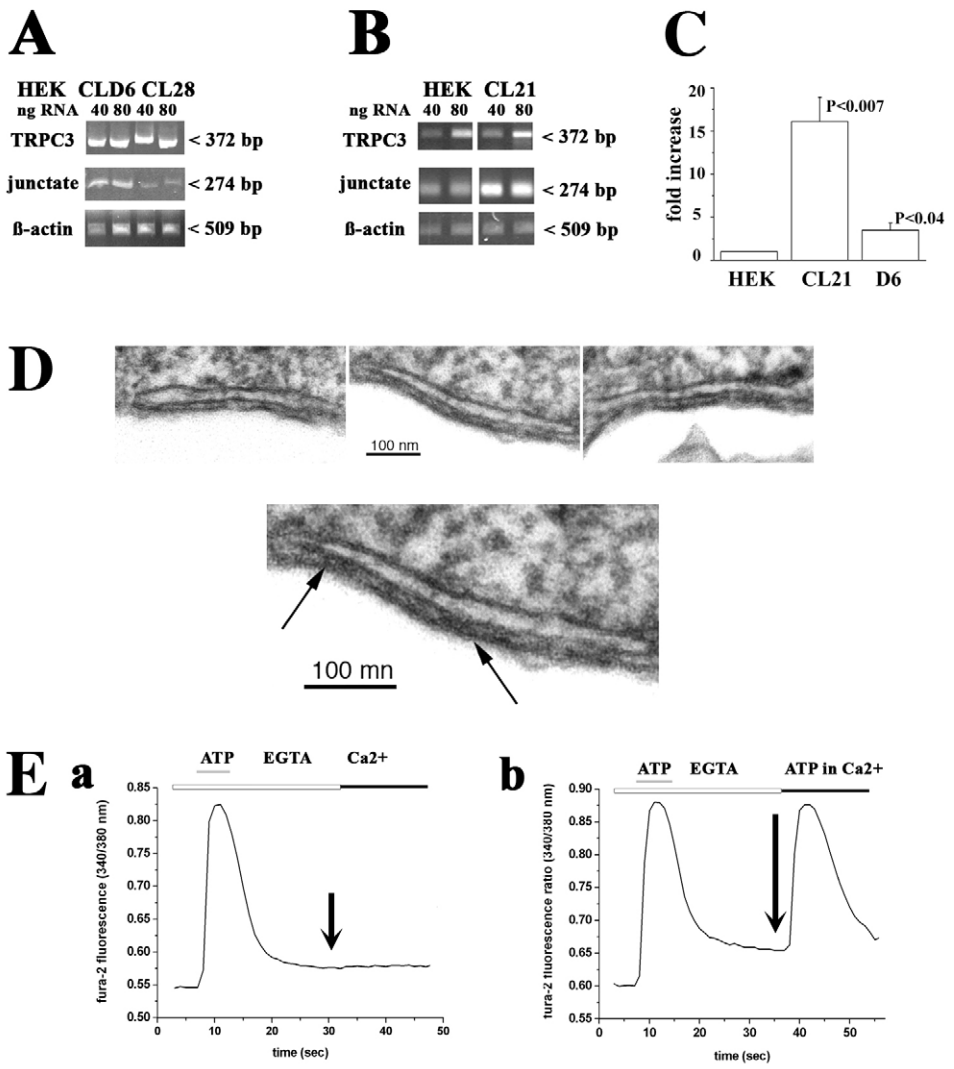

Fig. 3. Characteristics of HEK junctate and HEKT3 junctate overexpressing clones. Total RNA was extracted from HEK T3 and HEK T3-junctate clone D6 cells (**A**) or from control HEK293 and HEK293 junctate–YFP clone 21 cells (**B**) and converted into cDNA and amplified. (**C**) Real-time PCR analysis for quantification of junctate in HEK293 cells, clone 21 and clone D6; bars represent mean (±s.e.m.; n=4) fold increase of junctate transcript. (**D**) Peripheral couplings in HEK T3-junctate clone D6. Electron micrographs showing that the endoplasmic reticulum and plasma membrane form junctions (between arrows) of variable length. (**E**) Fura-2-loaded HEKT3 junctate clone D6 cells were stimulated as indicated. Small arrow shows addition of 2 mM Ca^{2+} (a). Large arrow shows addition of 2 mM Ca^{2+} plus 100 μM ATP (b). Results are representative of experiments carried out on 20 cells. ATP, 100 μM ATP; EGTA, Krebs-Ringer containing 0.5 mM EGTA; Ca^{2+}, Krebs-Ringer containing 2 mM Ca^{2+}; ATP in Ca^{2+}, 100 μM ATP in 2 mM Ca^{2+}.

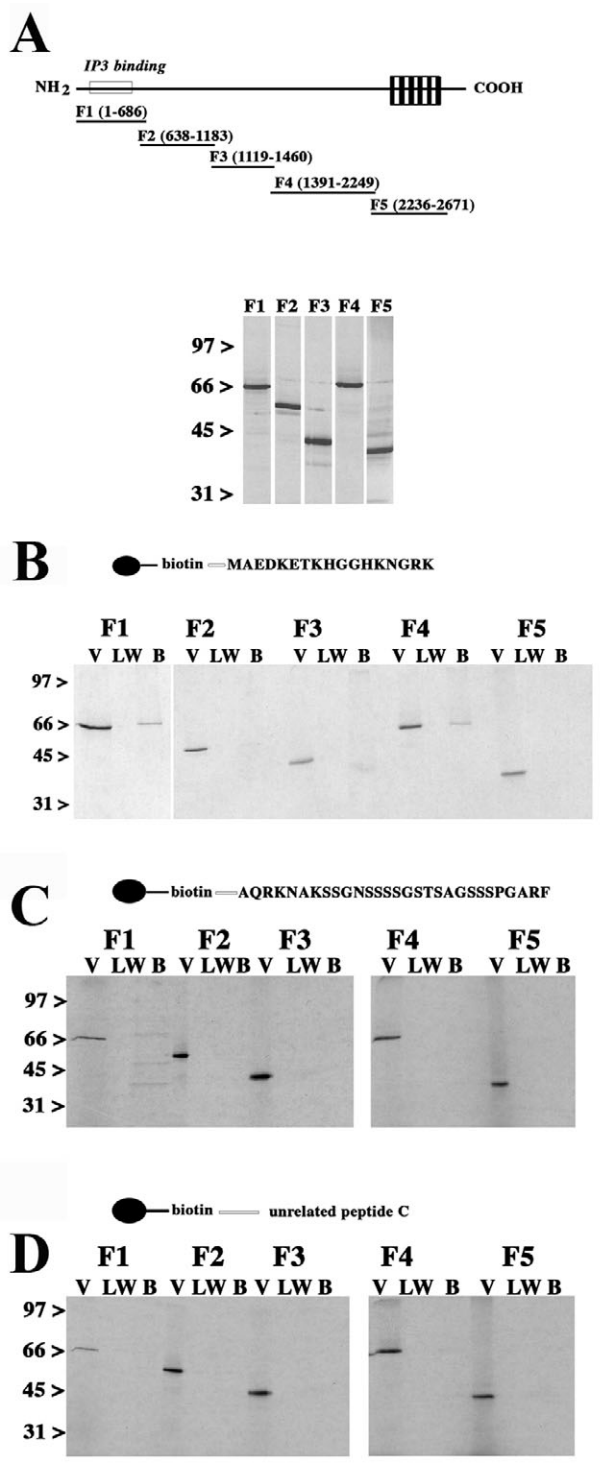

Fig. 4. Identification of the InsP_3R domains involved in the interaction with the N-terminus of junctate. (**A**) Schematic representation (top) and autoradiography (bottom) of an aliquot (5 µl) of the [^{35}S]Met-labelled overlapping in vitro transcribed and translated InsP_3R3 fragments separated by 10% SDS-PAGE. Streptavidin-coated beads coated with a biotinylated peptide corresponding to the N-terminus of junctate (**B**), aspartyl-β-hydroxylase (**C**) and an unrelated peptide (**D**) were incubated with the InsP_3R overlapping fragments F1–F5. Proteins present in the void (V), last wash (LW) and bound (B) to the beads were separated by 10% SDS-PAGE, gels were dried and exposed overnight to an X-ray film. Experiments were carried out at least four times with identical results.

used to activate the receptor in vitro (Ando et al., 2006). Fig. 5A shows that as the InsP_3 concentration in the binding solution increased from 0.3 µM to 10 µM, the intensity of the F1 band proportionally decreased (top panel); the addition of 1 µM InsP_3 caused a 20% decrease, whereas the addition of 10 µM InsP_3 decreased the binding between F1 and junctate by approximately 60%. Addition of 10 µM ATP (control) had no effect on the interaction between the two polypeptides (Fig. 5A, bottom panel). We further verified the effect of junctate on [^{3}H]InsP_3 binding by performing ligand-binding experiments in the presence of either the peptide encompassing the N-terminus of junctate or an unrelated peptide. Fig. 5B shows that the amount of InsP_3 bound (B_{max}) at low nanomolar concentrations was similar in the presence of either 50 µM junctate peptide or the unrelated peptide. In summary, these results show that junctate can interact directly with the domain of the InsP_3R that is involved in ligand binding. In the presence of InsP_3, the amount of F1 (residues 1–686 of the human InsP_3R3 isoform) bound to the N-terminus of junctate was significantly reduced. Since ligand binding was unaffected by the presence of the junctate N-terminal peptide, it follows that the affinity of the InsP_3R for its ligand InsP_3 is probably much higher than that for junctate.

Agonist-induced Ca^{2+} entry within junctate–YFP-expressing puncta

The results obtained using TIRF and electron microscopy indicate that junctate–YFP puncta correspond to cell domains endowed with stable peripheral couplings between the ER and the PM, which might form one of the anatomical sites responsible for Ca^{2+} entry via a conformational coupling mechanism. We next measured Ca^{2+} influx by monitoring Fura Red fluorescence changes in TIRF mode in puncta regions. Fura-Red-loaded HEK junctate–YFP cells were first observed by epifluorescence at 488 nm excitation (Fig. 6Ab), with the SRIC filter (Fig. 6Ac) to fix the correct focal plane to be used in TIRF mode, and subsequently the junctate–YFP puncta were visualized by exciting the cells with a Sapphire laser (Fig. 6Ad). Under these conditions the fluorescence resulting from Fura Red was virtually absent because the excitation and emission wavelength spectra of the Ca^{2+} indicator (λex, 410 nm; λem, 620 nm) did not overlap with those of YFP. Keeping the same focal plane fixed for YFP puncta observation, HEK junctate–YFP cells were then illuminated with a laser at 405 nm; at this wavelength, the Ca^{2+}-bound form of Fura Red was excited with an efficiency of approximately 70%, whereas there was virtually (<2%) no excitation of YFP. By using emission barrier filters (625 nm), we monitored the emission of Fura Red and thus were able to follow changes in $[Ca^{2+}]_i$ in regions within a space of 150 nm of the PM. Fig. 6B shows the changes in the fluorescent ratio caused by the addition of 100 µM ATP in the absence (dotted trace) and in the presence (continuous trace) of 2 mM extracellular Ca^{2+}, occurring within a punctuated junctate–YFP-containing area. In the presence of 2 mM extracellular Ca^{2+}, the kinetics and magnitude of the Ca^{2+} signal were clearly different from those observed in the presence of EGTA. In the presence of 2 mM Ca^{2+}, the signal had a rapid initial peak increase, remained elevated for a prolonged time period and then decayed non-linearly. In the presence of EGTA, the signal was smaller and showed an immediate linear decay. The peak Ca^{2+} component obtained in the presence of extracellular Ca^{2+} represents the change in Fura Red fluorescence due to Ca^{2+} entry. Although the mean peak increase in Fura Red fluorescence

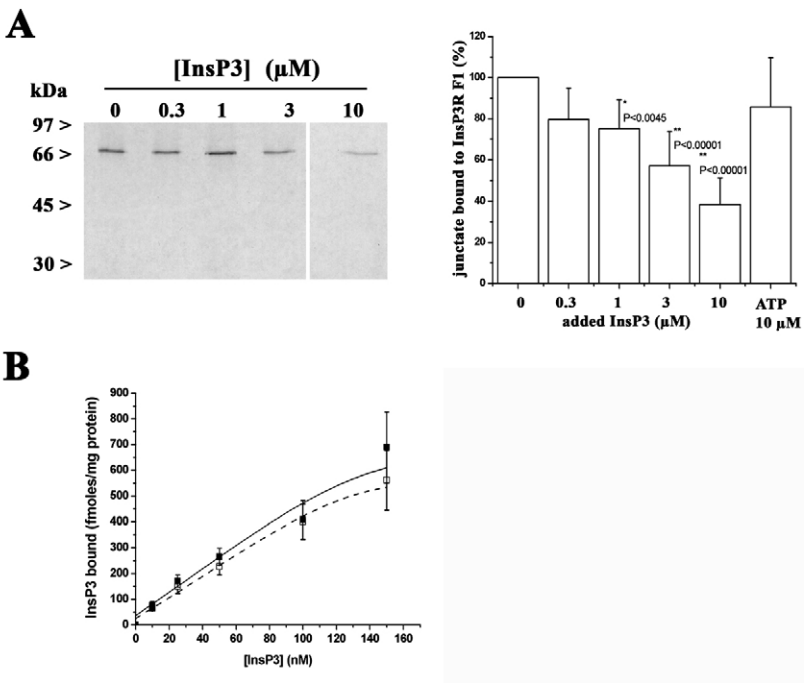

Fig. 5. The interaction between InsP_3R F1 and the peptide encompassing the N-terminus of junctate is influenced by InsP_3 but it does not significantly affect InsP_3 binding to microsomes from HEK293 cells. (**A**) Streptavidin-coated beads incubated with the biotinylated peptide encompassing the junctate N-terminus, were incubated with [^{35}S]Met in vitro transcribed and translated F1 peptide (residues 1–686 of the human InsP_3R3), in the presence of the indicated concentration of InsP_3 (0–10 μM) or 10 μM ATP (control). Bound proteins were eluted by incubating the beads with 5% SDS and boiling the samples for 5 minutes. The supernatant was separated by 10% SDS-PAGE, the gel was dried and exposed to an X-ray film. The intensity of the bands corresponding to F1 were quantified by densitometry using Bio-Rad GelDoc 2000 and are plotted in the lower panel of Fig. 2B. 100% represents the intensity of the F1 band obtained in the absence of competing InsP_3. Bars represent the mean ± s.e.m. of five measurements. (**B**) InsP_3 binding to microsomes from HEK293 cells in the presence of 50 μM N-terminal junctate peptide (closed squares) or in the presence of an unrelated peptide (open circles). Results show the mean amount of InsP_3 bound (fmoles/mg protein) ± s.e.m. of 4–8 determinations.

induced by 100 μM ATP in the presence of extracellular Ca^{2+} was significantly higher than that in the presence of EGTA, there was a remarkable variability of the data (Fig. 6C). Variability could theoretically depend on (1) subtle variations of the focal plane during recordings in TIRF mode; (2) different expression levels of juncate–YFP in the puncta, or (3) a combination of both. We excluded the first possibility because our TIRF set up was equipped with an on-line control of the focal plane, which avoids any focal drift, a crucial parameter during TIRF recordings. Since the fluorescence intensity of junctate–YFP puncta was quite heterogeneous (Fig. 6Ad), we analyzed the relationship between the peak Ca^{2+} signal increase and junctate–YFP fluorescence intensity (Fig. 6D,E). Although with some scatter, the data show a parallel increase in both parameters (Fig. 6D). Indeed, the relationship was linear with a good correlation (R=0.857) at low to intermediate juncate–YFP fluorescence levels (Fig. 6E), but the peak Ca^{2+} signal saturates in puncta exhibiting high levels of expression of juncate–YFP (Fig. 6D).

Discussion

In the present work, we studied the structural and functional relationship of a supramolecular complex involved in regulating Ca^{2+} homeostasis of non-muscle cells. Our results show that junctate forms distinct puncta in regions on or very close to the PM, whose size and distribution are unaffected by mobilization of calcium from an InsP_3-sensitive store. Puncta are associated with the appearance of ER–PM peripheral junctions. Interestingly, such junctions are endowed with regularly spaced electron-dense structures that bridge the gap between ER and PM. We propose that these peripheral junctions contain junctate–InsP_3R–TRPC3 complexes because their number is dependent on the co-expression of protein components of the complexes, namely junctate and the Ca^{2+}-entry channel TRPC3. Ca^{2+} imaging by TIRF microscopy demonstrates that puncta are domains in which agonist-activated Ca^{2+} entry occurs; the extent of Ca^{2+} entry correlates with the level of junctate expression.

Interaction of junctate with InsP_3R

An interesting observation arising from this study is that the N-terminus of junctate interacts with a domain on the InsP_3R3 involved in ligand binding (Maranto, 1994), making junctate a member of the group of proteins including IRBIT, RACK1, Homer, CaM, CaBP1 and TRPC3, which have been found to interact within residues 1–680 of the InsP_3R (Mikoshiba, 2007). The results of the pull-down assay are specific because no signals were detected in the Sepharose beads when we used an unrelated biotinylated peptide or when the pull down was carried out with a peptide derived from the N-terminus of aspartyl-β-hydroxylase/humbug, an alternative splice product of the gene encoding junctate, aspartyl-β-hydroxylase and junctin (Treves et al., 2009). The interaction of junctate with the InsP_3R is inhibited by InsP_3, the physiological ligand of the receptor. Such a result is reminiscent of that seen with IRBIT, the only other protein that binds to the InsP_3 binding domain on the InsP_3R to be displaced by InsP_3 (Ando et al., 2006). However, as opposed to IRBIT, junctate alters neither the K_D nor the B_{max} of InsP_3 binding, thus it does not act as a competitive inhibitor, but could be important in maintaining the structure of the InsP_3R macromolecular complex (Kiselyov et al., 2005) within the ER, a function similar to that attributed to 4.1N, another InsP_3R binding protein (Mikoshiba, 2007).

Peripheral coupling of HEK293 clones

The ‘conformational coupling’ hypothesis, one of the models proposed to explain Ca^{2+} entry, predicts an interaction between Ca^{2+}-entry channels and InsP_3Rs localized at ER–PM peripheral junctions (Irvine, 1990; Kiselyov et al., 2000; Berridge, 2004). Activation of such complexes may be triggered (1) by InsP_3 stimulation of a set of InsP_3R coupled to Ca^{2+}-entry channels within peripheral junctions or (2) by opening perijunctional InsP_3Rs leading to localized depletion of peri-junctional ER stores and subsequent switching on of store-operated channels. The organization and assembly of ER–PM peripheral junctions are crucial aspects that still remain to be elucidated to prove the

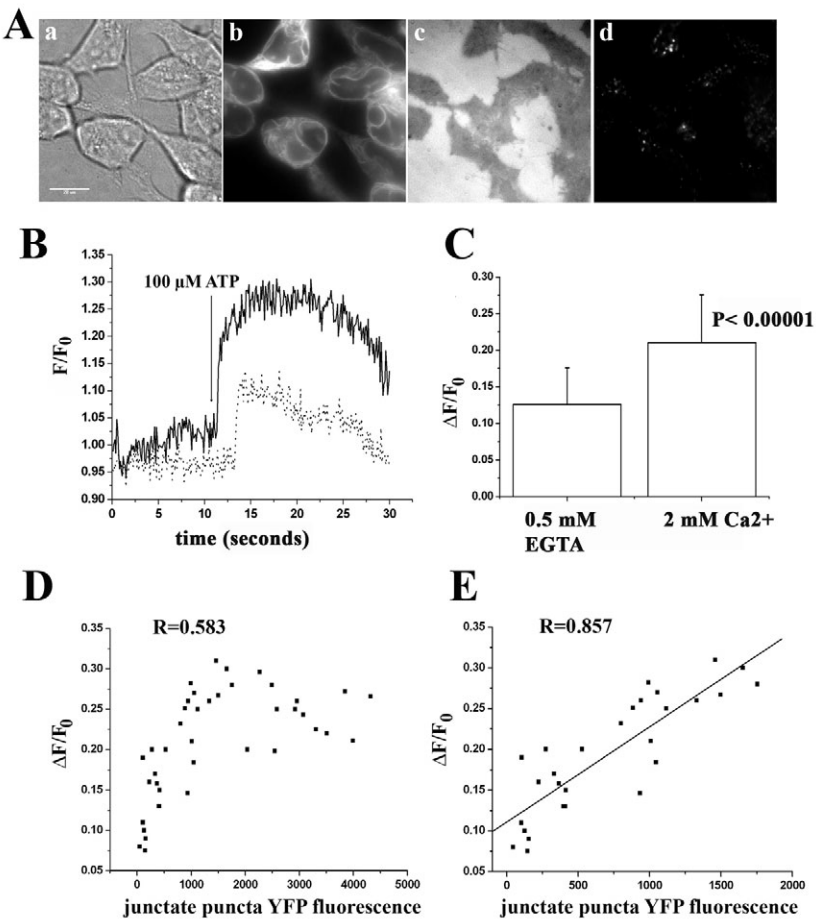

Fig. 6. Changes in $[Ca^{2+}]_i$ occur within domains of the plasma membrane enriched in junctate. (**A**) Fura-Red-loaded HEK junctate–YFP (clone 21) cells were visualized (a) by bright-field, (b) by epifluorescence, (c) with a surface reflection interference contrast filter and (d) by TIRF microscopy (488 nm excitation, 510 nm emission). Scale bar: 10 µm. (**B**) Changes in the intracellular Ca^{2+} concentration of junctate–YFP clone 21 cells were visualized by TIRF microscopy following the changes in fluorescence of Fura Red (405 nm excitation, 625/640 nm emission) within the YFP-positive puncta, induced by the addition of 100 µM ATP in Krebs-Ringer containing 0.5 mM EGTA (dotted line) or by the addition of 100 µM ATP in Krebs-Ringer containing 2 mM Ca^{2+} (continuous line). The traces in B show the change in the Ca^{2+}-dependent Fura Red fluorescence at 625 nm over time (ΔF, fluorescent value at any time point; F_o, fluorescence value at t=0). (**C**) Bar graph showing the mean peak increase (±s.d.) of Fura Red fluorescence induced by 100 µM ATP in the presence of 2 mM Ca^{2+} (n=30) or in the presence of 0.5 mM EGTA (n=28). (**D**,**E**) Linear regression analysis correlating YFP fluorescent intensity values to peak increase in Fura Red fluorescence ratio induced by 100 µM ATP in medium containing 2 mM Ca^{2+}. In D, linear regression was calculated using all YFP fluorescent intensity values whereas in E, the analysis was made including values within 0 and 2000 fluorescent intensity units. Fluorescence analysis was performed using the Metamorph software; statistical analysis including linear regression was performed using the Origin Microcal software.

validity of this model. In the present report, we investigated the ultrastructural characteristics of HEK293 cells stably expressing junctate and junctate plus TRPC3. These HEK293 clones have a high number of peripheral ER–PM junctions that are characterized by the presence of electron-dense structures bridging the 10 nm gap between the ER and PM. Interestingly, the size of the junctional gap fits with measurements carried out using different experimental approaches, which show that in the junctional area the ER and PM are separated by 11–14 nm (Varnai et al., 2007; Orci et al., 2009). The ultrastructural properties of peripheral couplings in our HEK293 clones are strikingly similar to those of differentiating BC_3H1 cells, in which ordered arrays of Ca^{2+} release units made up of ryanodine receptors and L-type Ca^{2+} channels are present (Protasi et al., 1997). Similar peripheral couplings have been observed in developing myotubes (Protasi et al., 1997), in *Xenopus* oocytes (Gardner and Grey, 1983) and in a number of mammalian cells (Levine, 2004). In *Xenopus* oocytes, the contact sites have been postulated to be involved in Ca^{2+} influx (Gardner and Grey, 1983). Although we do not know the exact identity of the electron-dense structures present in the ER–PM peripheral couplings in HEK293 clones, we suggest that they are the structural expression of the upregulation of the components of the supramolecular complex made up by junctate–YFP and TRPC3. The fluorescence of junctate–YFP was exploited to visualize expression of the protein in HEK293 clones by TIRF microscopy. The appearance of peripheral couplings is associated with the formation of puncta that are on or very close to the PM. The link between the appearance of peripheral couplings and the expression of junctate–YFP strongly suggests that the fluorescent puncta are subcellular domains endowed with ER–PM peripheral junctions. At first sight, the fluorescent puncta might seem to be more numerous and larger than the EM peripheral couplings; however, it should be kept in mind that the latter technique only looks at very thin sections. As to the actual size of the fluorescent puncta, these might be smaller than calculated by TIRF because of the spread function of the microscope. In addition, the cells analyzed by TIRF microscopy are living and adherent to the cover glass, and ER–PM junctions might be more abundant on the basal membrane facing the glass support compared with those on the apical membrane (Orci et al., 2009). The cells processed for EM imaging were resuspended and probably lost the polarity of the ER–PM interaction.

Peripheral couplings of HEK29 clones are stable

In TIRF mode we placed the laser beam at the most external region of the rear focal plane of the objective. Under this condition, the calculated penetration depth of the evanescent wave is up to 60 nm. Thus, the fluorescent signal of the puncta is derived from the 60 nm space adjacent to the internal face of the plasma membrane and might also be due to junctate–YFP localized in peri-junctional ER membranes. Nevertheless, bearing in mind the limitation of the spatial resolution of the TIRF, we suggest that puncta containing junctate–YFP represent Ca^{2+}-entry units that are probably different from those involved in SOCE induced by oligomerization of STIM1 with Orai1. The most important difference between the puncta induced by STIM1 and those containing junctate is that the appearance of the latter is not dependent on the level of Ca^{2+} load

in the ER. We also did not observe any change in size or localization of junctate-containing puncta upon addition of an InsP_3R-mobilizing agonist. A possible explanation of these data in line with the EM structural data is that junctate stabilizes the associations between the ER and PM.

Calcium signals in correspondence of stable ER–PM peripheral couplings

Ca^{2+} entry has recently been proposed to be secondary to the formation of ER–PM peripheral junctions mediated by the oligomerization of STIM1 and Orai1. However, this general scheme has been revisited on the basis of experiments demonstrating that activation of Ca^{2+} entry via Orai1 can occur in STIM1-deficient cells, and that the cytoplasmic domain of STIM1 is too small (Varnai et al., 2007) to bridge the 13-nm-wide junctional ER–PM gap (Orci et al., 2009). Our data suggest that Ca^{2+} entry can occur without de novo translocation of ER domains to subplasmalemma domains. Rather, agonist-activated Ca^{2+} entry can occur within junctate-containing puncta that do not change in size and location upon surface receptor activation of calcium release from the ER. The Ca^{2+} signal we recorded in TIRF mode contains a component derived from release from internal stores because it occurs in the presence of 0.5 mM EGTA. The additional Ca^{2+} signal component observed in the presence of extracellular Ca^{2+} is slower and must be derived from activation of Ca^{2+} entry. The latter component is probably mediated by a molecular complex modulated by junctate because it strongly correlates with the expression level of this protein in the puncta. In addition, we think that it is specific because it saturates at high levels of expression of junctate.

These results underlie the importance of junctate–InsP_3R–TRPC3 supramolecular complexes to form stable ER–plasma membrane peripheral couplings that might represent an anatomical site of agonist-activated Ca^{2+} entry.

Materials and Methods

In vitro synthesis of InsP_3R fragments and interaction with junctate

Fragments of InsP_3R3 were prepared as described (Tang et al., 2001). To verify the size of the polypeptides and translation efficiency, aliquots of the ^{35}S-labelled translation mixture were resolved by 10% SDS-PAGE. Gels were stained with Coomassie Brilliant Blue (CBB), dried and exposed to autoradiography. For pull-down studies, streptavidin-coated magnetic beads were washed three times with 10 mM HEPES pH 7.2, 150 mM NaCl (HEPES-NaCl) and incubated for 30 minutes at room temperature with a 10% blocking solution (Roche Applied Science) in HEPES-NaCl. Beads were rinsed with HEPES-NaCl and incubated with 10 μg/ml biotinylated synthetic peptides corresponding to (1) the N-terminus of junctate (MAEDKETKHGGHKNGRK), (2) the N-terminus of aspartyl-β-hydroxylase (AQRKNAKSSGNSSSSGSTSAGSSSPGARF) and (3) an unrelated biotinylated peptide, for 30 minutes at room temperature. Beads were washed three times with HEPES-NaCl and divided into five samples. To each Eppendorf tube containing biotinylated peptide bound to streptavidin beads, 5 μl ^{35}S-labelled in vitro synthesized polypeptides of the InsP_3R (F1–F5) were added. After incubation for 1 hour at room temperature, beads were spun down and unbound material (void) was retained. Pellets were washed four times with 1 ml HEPES-NaCl, after which 40 μl of 5% SDS were added to the pellets; mixtures were incubated for 5 minutes at 95°C, spun and the supernatants (bound) were retained. Proteins in the samples corresponding to void, last wash and bound were separated by 10% SDS-PAGE; after CBB staining, gels were dried and processed for autoradiography.

[^{3}H] InsP_3 binding

InsP_3 concentration-dependent binding studies were carried out on HEK293 microsomes (75 μg) in 100 mM KCl, 10 mM NaCl, 10 mM Tris–HCl, pH 7.5, with [^{3}H]Inositol-1,4,5-trisphosphate (Perkin Elmer; specific activity 0.001 mCi/ml) plus cold InsP_3 (Calbiochem) to give a final concentration of InsP_3 of 10, 25, 50, 100 and 150 nM, in the presence of 50 μM of an unrelated peptide or a synthetic peptide corresponding to the N-terminus of junctate. Values for non-specific binding were obtained by incubating microsomes with an excess (10 μM) unlabelled InsP_3. Samples were incubated for 30 minutes at 4°C, filtered through Whatman glass microfibre GFP filters by means of a Millipore Manifold filtering apparatus and the amount of radioactivity retained on the filters was determined by liquid scintillation counting.

HEK293 cell clones overexpressing junctate

HEK293 cells were transfected with the cDNA encoding junctate-EYFP (full-length junctate subcloned into the EYFP-C1 vector) using calcium phosphate. Stable clones (HEK junctate–YFP) were selected by adding G418 (final concentration 800 μg/ml) to the growth medium (DMEM + Earl's salts, containing 10% foetal bovine serum and penicillin-streptomycin). After 2 weeks in selective medium when they became visible, single clones were picked and expanded. For HEK clones overexpressing TRPC3 and junctate, the full-length junctate cDNA was subcloned into the *Hin*dIII site of the pcDNA 3.1/Hygro plasmid (Invitrogen life technologies). The construct was checked by sequencing and the plasmid was used to transfect a HEK293 cell line stably expressing TRPC3 (HEK T3 cells) (Zhu et al., 1998) using the ESCORT IV transfection reagent (Sigma, St Louis, MO) at a DNA: liposome ratio of 1:4, following the manufacturer's instructions. Stable clones (HEK T3–junctate) were selected by adding G418 and hygromycin (800 μg/ml and 200 μg/ml, respectively) to the growth medium (DMEM containing 10% foetal bovine serum, and penicillin-streptomycin). Three weeks after transfection, single clones were picked and expanded.

Analysis of gene expression by semi-quantitative and real-time RT-PCR

Total RNA was extracted from 2×10^6 HEK293, HEK Junctate–YFP and clone HEK T3–junctate cells (Qiagen, Basel, Switzerland) and treated with Deoxyribonuclease I (DNaseI) (Invitrogen, Carlsbad, CA). After reverse transcription using 1000 ng RNA and the Moloney Murine Leukemia Virus Reverse Transcriptase (M-MLV RT) (Invitrogen), cDNA was amplified by quantitative real-time PCR in the ABI PrismTM7700 using the TaqMan® technology. Commercially available exon-intron junction-designed primers for human GAPDH and InsP_3R3 (Applied Biosystems, Foster City, CA) were used. Gene expression was normalized using self-GAPDH as reference and calculated as a fold increase compared with gene expression in HEK293 cells. In the case of junctate, real-time RT-PCR was carried out using SYBR Green technology (fast SYBR green master mix, Applied Biosystems) and the following primers: junctate forward, 5′-ATGGAGGACACAAGAATGGGA-3′ and reverse, 5′-CCAAACGACAGCTACAGATGT-3′.Gene expression was normalized using self-TATA box binding protein (TBP) as reference using the same technique and the following primers: forward, 5′-GCCATAAGGCATCATTGGAC-3′ and reverse, 5′-AACAACAGCCTGCCACCTTA-3′. For semiquantitative RT-PCR, total RNA was isolated from HEK cell clones using ULTRASPEC reagent (Biotecx) and transcribed into cDNA using a kit from Roche Diagnostics, oligo- (dT) as primers and AMV Reverse Transcriptase as previously described (Treves et al., 2004). RT PCR was carried out as previously described for junctate (Treves et al., 2004) and using the following primers and conditions for TRPC3: forward, 5′-ATG CTG CTT TTA CCA CTG TAG-3′ and reverse 5′-TCC TTC TGC ATT TGG GAA A-3′ (95°C for 5 minutes, followed by 35 cycles of 45 seconds 94°C, 45 seconds 51°C, 45 seconds 72°C; followed by extension at 72°C for 3 minutes); β-actin forward, 5′-TGA CGG GGT CAC CAC-3′ and reverse, 5′-CTA GAA GCA TTG CGG T-3′ (95°C for 5 minutes, followed by 25 cycles of 30 seconds 94°C, 45 seconds 49°C, 45 seconds 72° followed by extension at 72°C for 3 minutes). PCR products were separated and the DNA bands visualized by ethidium bromide staining.

Electrophoresis, western blotting and immunofluorescence

SDS-PAGE, protein transfer onto nitrocellulose and immunostaining were performed as previously described (Treves et al., 2000; Treves et al., 2004). Blots were probed with a polyclonal goat anti-InsP_3R1, anti-InsP_3R2 and or anti-InsP_3R3 antibodies and anti-β-tubulin (Santa Cruz) or mouse anti-GFP (Roche Applied Science) followed by peroxidase-conjugated secondary antibodies. The immunopositive bands were visualized by chemiluminescence using the Super Signal West Dura kit from Thermo Scientific. For immunofluorescence, glass coverslip grown HEK293 junctate–YFP clone 21 cells were fixed with ice-cold acetone:methanol (1:1) for 20 minutes, rinsed twice with phosphate-buffered saline (PBS) and blocked with 10% blocking buffer (Roche Applied Science) for 60 minutes at room temperature. Coverslips were incubated with polyclonal goat anti-InsP_3R3 antibody (Santa Cruz); after 60 minutes, coverslips were rinsed three times for 5 minutes with PBS and incubated with rabbit anti-goat DyLighte Fluor-405 (400 nm excitation, 420 nm emission) (Rockland, Gilbertsville, PA) and rabbit anti-GFP Alexa Fluor 488. After 60 minutes, coverslips were extensively washed and mounted in glycerol mounting medium. Fluorescence was visualized by TIRF microscopy as described in the next section, by exciting at 488 nm (Sapphire Laser) to visualize GFP fluorescence, and at 405 nm using a laser from Coherent Laboratories. DyLighte Fluor-405 fluorescence was visualized using a BrightLine CH 427 filter (AHF Analysentechnir, Tübingen, Germany). Colocalization analysis of junctate and InsP_3R3 was performed using the colocalization application included in the Metamorph 5.7.4 software package.

TIRF and electron microscopy

For TIRF microscopy, HEK junctate–YFP stable clones or HEK293 transiently transfected with a plasmid encoding a GFP fusion protein targeted to the ER (SScalEGFP was a gift from Hans-Peter Hauri, Biozentrum, Basel University, Switzerland) were grown on a 0.17-mm-thick glass coverslip. Cells were imaged

with a Nikon Eclipse TE2000-E fluorescent microscope equipped with an oil immersion CFI Plan Apochromat 100× TIRF objective (1.49 numerical aperture). Changes in fluorescence were detected by exciting at 488 nm and recording the emission at 510 nm via an electron multiplier C9100-13 Hamamatsu CCD camera. The focal plane corresponding to the glass coverslip cell adhesion site was selected using the SRIC filter; this focal plane was maintained throughout the experiment, using the Perfects Focus System. Cells were stimulated with Krebs-Ringer containing 2 mM Ca^{2+} for 5 seconds, followed by a 10 second stimulation with 100 μM ATP. Analysis of the size and shape of fluorescent puncta was performed with the Integrated morphometric analysis application included in the Metamorph 5.7.4 software package. Movement analysis was performed on the acquired stacks using Metamorph 7.5 software. To track movement, individual regions of interest were selected, subjected to a 2×2 low-pass filter, after which threshold values were set. Movement was tracked on selected fluorescent puncta using the 'track object' software included in the Metamorph 7.5 software package.

For electron microscopy, HEK293 cell clones were gently detached from tissue culture dishes, rinsed with PBS, fixed in 3% glutaraldehyde in PBS and pelleted. Cells were maintained in fixative for several days. Pellets were post-fixed in osmium tetraoxide, en-bloc 'stained' in uranyl acetate and embedded. Thin sections showed 1–200 profiles of cells per section, cut in random orientations. Sections were stained in solutions containing uranyl acetate and lead and examined in a Philips 410 electron microscope.

$[Ca^{2+}]_i$ measurements

For measurement of cell populations, HEK cells were loaded with 5 μM Fura-2 AM in Krebs-Ringer buffer containing 2 mM external calcium. After 30 minutes at 37°C, cells were rinsed and changes in Fura-2 fluorescence were monitored by following the changes in fluorescence at 340 and 380 nm (excitation) and 515 nm (emission) with a Perkin Elmer LS6 spectrofluorimeter equipped with a magnetically controlled thermostat chamber. Cells (1×10^6 cells/ml) were stimulated either with thapsigargin (400 nM) or with 100 μM ATP in Krebs-Ringer containing 0.5 mM EGTA; in some experiments 0.5 mM Ca^{2+} was added back to stimulate Ca^{2+} influx.

Single-cell ratiometric Fura-2 Ca^{2+} measurements were performed as previously described (Treves et al., 2004). For single-cell Ca^{2+} measurements by TIRF microscopy, junctate–YFP cells grown on glass coverslips were loaded with 5 μM Fura Red AM at 37°C for 30 minutes in Krebs-Ringer containing 2 mM Ca^{2+}. Coverslips were mounted in a thermostat perfusion chamber and the focal plane corresponding to the glass coverslip and cell membrane contact site was identified using the Surface Refection Interference Contrast (SRIC) filter and fixed with the Perfect Focus System. YFP fluorescent puncta were visualized by illuminating the cells with a Sapphire laser and monitoring fluorescence at 510 nm; maintaining the same focal plane changes in the $[Ca^{2+}]$ measurements were monitored by illuminating the cells with a 405 nm laser and following the emission at 625–640 nm using a brightline HC 625/26 cut-off filter (AHF Analysentechnir). Images were acquired in TIRF mode every 100 mseconds using a Nikon Eclipse TE2000-E fluorescent microscope equipped with an oil immersion CFI Plan Apochromat 100× TIRF objective as described above.

Statistical analysis

Statistical analysis was performed using the Student's *t*-test for unpaired samples; means were considered statistically significant when $P<0.05$. Linear regression analysis and statistical analysis was performed using the statistics package included in the Origin 6.0 (Micorcal) software.

We would like to thank Olivier Pertz for help with the particle tracking, Serge Summermatter for help with the real-time RT-PCR, Anne-Sylvie Monnet for expert technical assistance and Nosta Glaser for electron microscopy support, as well as Alex Eberle for the bitotinylated unrelated peptide. This work was supported by grants from Ministero Universita e Ricerca scientifica e Tecnologica 40%, F.I.R.B. RBAUO01ERMX, by the Department of Anaesthesia, Basel University Hospital and by National Institutes of Health grants NIH RO1 HL48093 to C.F.A. and ROI DK081654 to M.X.Z. Deposited in PMC for release after 12 months.

Supplementary material available online at
http://jcs.biologists.org/cgi/content/full/123/23/4170/DC1

References

Ando, H., Mitzutani, A., Kiefer, H., Tsuzurugi, D., Michikawa, T. and Mikoshiba, K. (2006). IRBIT suppresses IP3 receptor activity by competing with IP3 for the common binding site on the IP3 receptor. *Mol. Cell* **22**, 795-806.

Berridge, M. J. (1995). Capacitative calcium entry. *Biochem. J.* **312**, 1-11.

Berridge, M. J. (2004). Conformational coupling: a physiological calcium entry mechanism. *Sci. STKE* **243**, pe33.

Dellis, O., Dedos, S. G., Tovey, S. C., Ur-Rahman, T., Dubel, S. J. and Taylor, C. W. (2006). Ca^{2+} entry through plasma membrane IP3 receptors. *Science* **313**, 229-233.

Eisner, D. A. and Trafford, A. W. (2009). What is the purpose of the large sarcolemmal calcium flux on each heartbeat? *Am. J. Physiol. Heart. Circ. Physiol.* **297**, H493-H494.

Feske, S., Giltnane, J., Dolmetsch, R., Staudt, L. M. and Rao, A. (2001). Gene regulation mediated by calcium signals in T lymphocytes. *Nat. Immunol.* **2**, 316-324.

Franzini-Armstrong, C. and Jorgensen, A. O. (1994). Structure and development of E-C coupling units in skeletal muscle. *Annu. Rev. Physiol.* **56**, 509-534.

Franzini-Armstrong, C. and Protasi, F. (1997). Ryanodine receptors of striated muscles: a complex channel capable of multiple interactions. *Physiol. Rev.* **77**, 699-729.

Gardner, D. M. and Grey, R. D. (1983). Membrane junctions in Xenopus eggs: their distribution suggests a role in calcium regulation. *J. Cell Biol.* **96**, 1159-1163.

Gwack, Y., Srikanth, S., Feske, S., Cruz-Guilloty, F., Oh-hora, M., Neems, D. S., Hogan, P. G. and Rao, A. (2007). Biochemical and functional characterization of orai proteins. *J. Biol. Chem.* **282**, 16232-16243.

Gwozdz, T., Dutko-Gwozdz, J., Zarayskiy, V., Peter, K. and Bolotina, V. M. (2008). How strict is the correlation between STIM1 and Orai1 expression, puncta formation, and I_{CRAC} activation? *Am. J. Physiol. Cell Physiol.* **295**, C1133-C1140.

Hofer, A. M., Fasolato, C. and Pozzan, T. (1998). Dynamic properties of an inositol 1,4,5-trisphosphate- and thapsigargin-insensitive calcium pool in mammalian cell lines. *J. Cell Biol.* **136**, 355-366.

Huang, G. N., Zeng, W., Kim, J. Y., Yuan, J. P., Han, L., Muallem, S. and Worley, P. F. (2006). STIM1 carboxyl-terminus activates native SOC, I_{CRAC} and TRPC1 channels. *Nat. Cell Biol.* **8**, 1003-1010.

Irvine, R. F. (1990). Quantal' Ca^{2+} release and the control of Ca^{2+} entry by inositol phosphates- a possible mechanism *FEBS Lett.* **263**, 5-9.

Kiselyov, K. I., Shin, D. M., Wang, Y., Pessah, I. N., Allen, P. D. and Muallem, S. (2000). Gating of store-operated channels by conformational coupling to ryanodine receptors. *Mol. Cell.* **6**, 421-431.

Kiselyov, K. I., Kim, J. Y., Zeng, W. and Muallem, S. (2005). Protein-protein interaction and functionTRPC channels. *Pflugers Arch.* **451**, 116-124.

Levine, T. (2004). Short-range intracellular trafficking of small molecules across endoplasmic reticulum junctions. *Trends Cell Biol.* **14**, 483-490.

Liou, J., Kim, M. L., Heo, W. D., Jones, J. T., Myers, J. W., Ferrell, J. E. and Meyer, T. (2005). STIM1 is a Ca^{2+} sensor essential for Ca^{2+}-store depletion-triggered Ca^{2+} influx. *Curr. Biol.* **15**, 1235-1241.

Luik, R. M., Wang, B., Prakriya, M., Wu, M. M. and Lewis, R. S. (2008). Oligomerization of STIM1 couples ER calcium depletion to CRAC channel activation. *Nature* **454**, 538-542.

Maranto, A. R. (1994). Primary structure, ligand binding, and localization of the human type 3 inositol 1,4,5-trisphosphate receptor expressed in intestinal epithelium. *J. Biol. Chem.* **269**, 1222-1230.

Mikoshiba, K. (2007). IP_3 receptor/Ca^{2+} channel: from discovery to new signalling concepts. *J. Neurochem.* **102**, 1426-1446.

Orci, L., Ravazzola, M., Le Coadic, M., Shen, W. W., Demereux, N. and Cosson, P. (2009). From the Cover: STIM1-induced precortical and cortical subdomains of the endoplasmic reticulum. *Proc. Natl. Acad. Sci. USA* **106**, 19358-19362.

Parekh, A. B. and Putney, J. W., Jr (2005). Store-operated calcium channels. *Physiol. Rev.* **85**, 757-810.

Park, C. Y., Hoover, P. J., Mullins, F. M., Bachhawat, P., Covington, E. D., Raunser, S., Walz, T., Garcia, C., Dolmetsch, R. E. and Lewis, R. S. (2009). STIM1 clusters and activates CRAC channels via direct binding of a cytosolic domain to Orai1. *Cell* **136**, 876-890.

Penna, A., Demuro, A., Yeromin, A. V., Zhang, S. L., Safrina, O., Parker, I. and Cahalan, M. D. (2008). The CRAC channel consists of a tetramer formed by Stim-induced dimerization of Orai dimers. *Nature* **456**, 116-120.

Prakriya, M., Feske, S., Gwack, Y., Srikanth, S., Rao, A. and Hogan, P. G. (2006). Orai1 is an essential pore subunit of the CRAC channel. *Nature* **443**, 230-233.

Protasi, F., Franzini-Armstrong, C. and Flucher, B. E. (1997). Coordinated incorporation of skeletal muscle dihyropyridine receptors in peripheral couplings of BC3H1 cells. *J. Cell Biol.* **137**, 859-870.

Putney, J. W., Jr (2007). New molecular players in capacitative Ca^{2+} entry. *J. Cell Sci.* **120**, 1959-1965.

Spassova, M. A., Soboloff, J., He, L. P., Xu, W., Dziadek, M. A. and Gill, D. L. (2006). STIM1 has a plasma membrane role in the activation of store-operated Ca^{2+} channels *Proc. Natl. Acad. Sci. USA* **103**, 4040-4045.

Stathopulos, P. B., Li, G. Y., Plevin, M. J., Ames, J. B. and Ikura, M. (2006). Stored Ca^{2+} depletion-induced oligomerization of STIM1 via the EF-SAM region: An initiation mechanism for capacitive Ca^{2+} entry. *J. Biol. Chem.* **281**, 35855-35862.

Takeshima, H., Komazaki, S., Nishi, M., Iino, M. and Kangawa, K. (2000). Junctophilins: a novel family of junctional membrane complex proteins. *Mol. Cell* **6**, 11-22.

Tang, J., Lin, Y., Zhang, Z., Tikunova, S., Birnbaumer, L. and Zhu, M. X. (2001). Identification of common binding sites for calmodulin and inositol 1,4,5-trisphosphate receptors on the carboxyl termini of TRP channels. *J. Biol. Chem.* **276**, 21303-21310.

Treves, S., Feriotto, G., Moccagatta, L., Gambari, R. and Zorzato, F. (2000). Molecular cloning, expression, functional characterization, chromosomal localization, and gene structure of junctate, a novel integral calcium binding protein of sarco(endo)plasmic reticulum membrane. *J. Biol. Chem.* **275**, 39555-39568.

Treves, S., Franzini-Armstrong, C., Moccagatta, L., Arnoult, C., Grasso, C., Schrum, A., Ducreux, S., Zhu, M. X., Mikoshiba, K., Girard, T. et al. (2004). Junctate is a key element in calcium entry induced by activation of InsP3 receptors and/or calcium store depletion. *J. Cell Biol.* **166**, 537-548.

Treves, S., Vukcevic, M., Maj, M., Thurnheer, R., Mosca, B. and Zorzato, F. (2009). Minor sarcoplasmic reticulum membrane components that modulate excitation-contraction coupling in striated muscles. *J. Physiol.* **587**, 3071-3079.

Van Rossum, D. B., Patterson, R. L., Kiselyov, K., Barrow, R. K., Gill, D. L. and Snyder, S. H. (2004). Agonist-induced Ca^{2+} entry determined by inositol 1,4,5-trisphosphate recognition. *Proc. Natl. Acad. Sci. USA* **101**, 2323-2327.

Varnai, P., Toth, B., Toth, D. J., Hunyady, L. and Balla, T. (2007). Visualization and manipulation of plasma membrane-endoplasmic reticulum contact sites indicates the presence of additional molecular components within the STIM1-Orai1 complex. *J. Biol. Chem*. **282**, 29678-29690.

Vazquez, G., Wedel, B. J., Bird, G. St J., Joseph, S. K. and Putney, J. W., Jr (2002). An inositol 1,4,5-trisphospate receptor-dependent cation entry pathway in DT40 B lymphocytes. *EMBO J.* **21**, 4531-4538.

Vig, M., Beck, A., Billingsley, J. M., Lis, A., Parvez, S., Peinelt, C., Koomoa, D. L., Soboloff, J., Gill, D. L., Fleig, A. et al. (2006). CRACM1 multimers form the ion-selective pore of the CRAC channel. *Curr. Biol.* **16**, 2073-2079.

Weisleder, N., Takeshima, H. and Ma, J. (2008). Immuno-proteomic approach to excitation-contraction coupling in skeletal and cardiac muscle: molecular insights revealed by the mitsugumins. *Cell Calcium* **43**, 1-8.

Wu, M. M., Buchanan, J., Luik, R. M. and Lewis, R. S. (2006). Ca^{2+} store depletion causes STIM1 to accumulate in ER regions closely associated with the plasma membrane. *J. Cell Biol*. **174**, 803-813.

Wu, M. M., Luik, R. M. and Lewis, C. S. (2007). Some assembly required: constructing the elementary units of store-operated Ca^{2+} entry. *Cell Calcium* **42**, 163-172.

Yeromin, A. V., Zhang, S. L., Jiang, W., Yu, Y., Safrina, O. and Cahalan, M. D. (2006). Molecular identification of the CRAC channel by altered ion selectivity in a mutant of Orai. *Nature* **443**, 226-229.

Zhang, S. L., Yu, Y., Roos, J., Kozak, J. A., Deerinck, T. J., Ellisman, M. H., Stauderman, K. A. and Cahalan, M. D. (2005). STIM1 is a Ca^{2+} sensor that activates CRAC channels and migrates from the Ca^{2+} store to the plasma membrane. *Nature* **437**, 902-905.

Zhu, M. X., Jiang, M. and Birnbaumer, L. (1998). Receptor-activated Ca^{2+} influx via human Trp3 stably expressed in human embryonic kidney (HEK)293 cells. *J. Biol. Chem*. **273**, 133-142.

Journal of Cell Science